Variable temperature Raman microscopy as a nanometrology tool for graphene layers and graphene-based devices

I. Calizo
Nano-Device Laboratory, Department of Electrical Engineering, University of California—Riverside, Riverside, California 92521

F. Miao, W. Bao, and C. N. Lau
Department of Physics and Astronomy, University of California—Riverside, Riverside, California 92521

A. A. Balandin[a)]
Nano-Device Laboratory, Department of Electrical Engineering, University of California—Riverside, Riverside, California 92521

(Received 15 May 2007; accepted 24 July 2007; published online 15 August 2007)

Raman microscopy of graphene was carried out over the temperature range from 83 to 373 K. The number of layers was independently confirmed by the quantum Hall measurements and atomic force microscopy. The values of the temperature coefficients for the *G* and 2D-band frequencies extracted from Raman spectra of the single-layer graphene are $-(1.6\pm0.2)\times10^{-2}$ cm^{-1}/K and $-(3.4\pm0.4)\times10^{-2}$ cm^{-1}/K, respectively. The *G* peak temperature coefficients of the bilayer graphene and bulk graphite are $-(1.5\pm0.06)\times10^{-2}$ cm^{-1}/K and $-(1.1\pm0.04)\times10^{-2}$ cm^{-1}/K, respectively. The results are important for the application of Raman microscopy as a nanometrology tool for the graphene-based devices operating at various temperatures. © *2007 American Institute of Physics*. [DOI: 10.1063/1.2771379]

Since its recent micromechanical isolation and measurements by Novoselov *et al.*,[1,2] graphene has attracted major attention from the physics and device research communities.[1–8] In addition to the wealth of the two-dimensional (2D) electron gas physics it reveals, graphene is a promising material for the electronic applications beyond the conventional complementary metal-oxide semiconductor (CMOS) technology. Geim and Novoselov[9] suggested that the band gap $\Delta E_G \sim 0.3$ eV can be induced in bilayer graphene and engineered in the single-layer graphene by spatial confinement or the lateral superlattice-type potential. The energy dispersion of graphene and large Fermi velocity V_F results in the substantial confinement gaps in the graphene ribbons on the order of ΔE_G (eV) $\sim hV_F/(4\pi d) \sim 1/d$ (nm), where h is the Planck constant and d is the width of the graphene ribbon.[9–12] Another important feature of graphene, which enhances its chances for being the beyond-CMOS material, is its extremely high carrier mobility of $\sim 15\,000$ cm^2 V^{-1} s^{-1} at room temperature.[1–3]

It was recently demonstrated that Raman spectroscopy can serve as a convenient technique for identifying graphene.[13,14] Ferrari *et al.*[13] studied the evolution of the 2D band Raman signatures with the addition of each extra layer of graphene and explained it with the double-resonance model. Gupta *et al.*[14] have shown that the *G* peak position ω_G is sensitive to the number of layers n, i.e., $\omega_G \sim 1/n$. The Raman spectroscopy studies of graphene[13–16] reported to date were limited to the room temperature. In order to expand the use of Raman spectroscopy as a nanometrology tool for the graphene-based devices, one has to investigate the change in the Raman signatures of graphene with temperature. This is essential for graphene-based devices, since the application of electric bias and gate voltages results in the device self-heating. In addition, the graphene-device characterization is often carried at low temperature. Thus, one needs to know the change in the *G* and 2D peak positions and shape with temperature in order to separate them from the changes due to the variations in the number of graphene layers. Although the thermal conductivity of graphene is expected to be high, there are always thermal resistances associated with the contacts and interfaces between different materials,[17,18] which may lead to the local temperature increase due to excitation or bias affecting the Raman spectrum.[19] The nanoribbons made of graphene for inducing the band gap may also deteriorate the thermal conductivity via the phonon-boundary scattering and phonon confinement.[20,21] These considerations provided an additional motivation for the temperature study of the graphene Raman signatures.

In this letter, we report the variable temperature spectroscopic Raman microscopy of the single-layer graphene (SLG) and bilayer graphene (BLG) deposited on silicon substrates for fabrication of the graphene-based devices. SLG and BLG were obtained by micromechanical cleavage of bulk graphite using the process outline in Refs. 1 and 2. Before performing the micro-Raman spectroscopy we carried out transport studies to confirm the quality of graphene and verify the number of layers. To characterize the graphene layers and devices, we attached the electrodes to a number of SLG and BLG using the standard nanofabrication techniques (with the drain-source separation of $1-5$ μm). The electrical measurements were performed at low temperature in a sorption pumped ^{3}He refrigerator.

A typical piece of graphene selected for fabrication is shown in Fig. 1(a). Figure 1(b) shows a characteristic linear-response conductance g_m of the graphene device as a function of the gate voltage V_g, which is used to tune the density of the charge carriers n_s in graphene. Assuming a parallel

a)Author to whom correspondence should be addressed; electronic mail: balandin@ee.ucr.edu

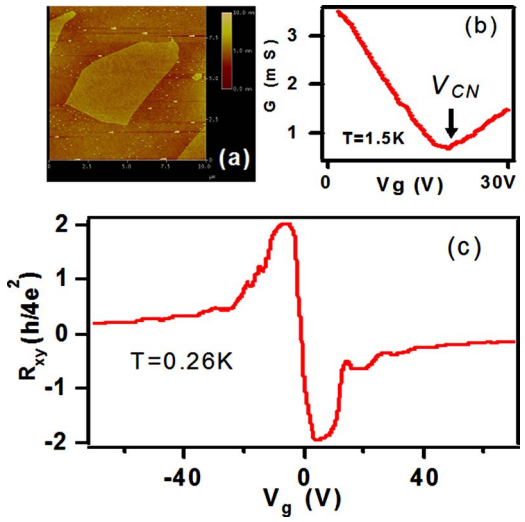

FIG. 1. (a) Atomic force microscopy image of the graphene layer used for the device fabrication, (b) Electrical conductance of the graphene device as a function of the applied gate bias, (c) Hall resistance of the graphene device as a function of the gate bias. Note that the value of the plateau confirms the relativistic band structure and selection of SLG.

plate capacitance between graphene and the back gate, we estimate n_s/V_g to be $\sim 7\times 10^{10}$ cm^{-2}/V. At the charge neutrality point V_{CN}, the device conductance attains its minimum. In an ideal graphene, this corresponds to nominally zero carrier density, where transport occurs entirely through the evanescent modes.[22] Away from V_{CN}, g_m increases linearly with V_g, which corresponds to the "electron-doped" and "hole-doped" regimes. The carrier mobility in the devices can be estimated from the slope of g_m-V_g curve using the Drude definition $\mu=\sigma/n_s e$ (here σ is the electric conductivity and e is the electron charge). For our devices we obtained $\mu\sim 8000-15\,000$ cm^2/V s, which attest to the material quality. Additional characterization was provided by the quantum Hall measurements at 8 T magnetic field. Figure 1(c) shows that the transverse resistance R_{xy} exhibits plateau at $h/(N+\frac{1}{2})\nu e^2$, where h is Planck's constant, ν accounts for spin and valley degeneracies ($\nu=4$ for graphene), and $N=0,\pm 1,\pm 2,\ldots$ is an integer. In sharp contrast to the standard quantum Hall quantization at $h/N\nu e^2$, the anomalous "half-integer" plateau is a unique signature of the relativistic band structure of graphene. The latter clearly establishes our selection of SLG for the present study.

The Raman microscopy was carried out using the Renishaw instrument. The spectra were excited by the 488 nm visible laser. A Leica optical microscope with 50× objective was used to collect the backscattered light from the graphene samples. The Rayleigh light was rejected by the holographic notch filter with a 160 cm^{-1} cutoff frequency for 488 nm excitation. The graphene temperature was changed using the cold-hot cell with the step of 10±0.1 K.

We varied the temperature of the sample in the range from 83 to 373 K and recorded Raman spectra at 10 K intervals. Both G and 2D peaks for SLG and BLG shift toward the lower frequency with the increasing temperature. The same trend was observed for the highly oriented pyrolytic graphine (HOPG), which we used as a reference sample. One can introduce the G (or 2D) mode temperature coefficient $\chi_{G,2D}$ through the expression for the peak frequency $\omega_{G,2D}=\omega'_{G,2D}+\chi_{G,2D}T$, where $\omega^0_{G,2D}$ is the frequency of the G(2D) peak when the absolute temperature T extrapolated to 0 K.

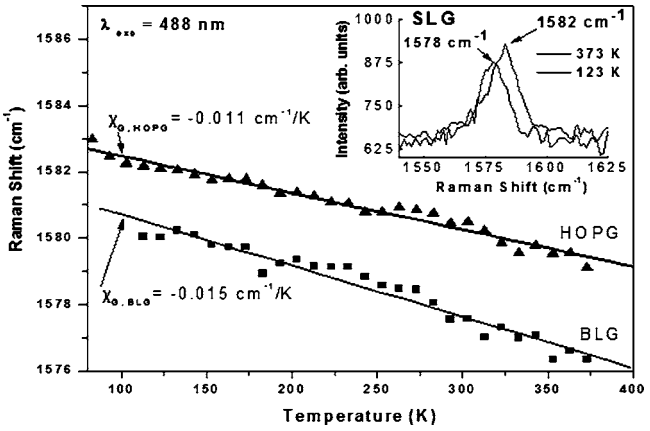

FIG. 2. Temperature dependence of the G peak position for BLG and HOPG. The inset shows the shape of the G peak and its shift for SLG.

The change of the Raman shift with temperature is a manifestation of the anharmonic potential constants, the phonon occupation number, and the thermal expansion of the graphene two-dimensional lattice.[23]

Figure 2 presents the temperature dependence of the G peak position for BLG and HOPG. The inset shows the G peak shape and position for SLG at two temperatures. The extracted G-mode temperature coefficient χ_G for SLG, BLG, and HOPG are listed in Table I. The observed linear trend for the G peak temperature dependence is consistent with the reports for other carbon-based materials. Ci *et al.*[24] observed the linear trend for χ of the radial breathing mode and the tangential stretching mode in the spectra from the double-wall carbon nanotubes in the $T=70-650$ K range. No deviation from the linear dependence was detected for the D and D^* peaks in the spectra from cardor nanotubes active carbon.[25] The nonlinear term in the temperature coefficient for Raman peaks from diamond only appears at the high end of the temperature $T=293-1850$ K range.[26] The comparison of graphene with other carbon materials is of interest because they consist of the same atoms but differ by either the type of sp hybridization or dimensionality.

In Figs. 3(a) and 3(b) we show the change in 2D feature in the Raman spectrum from SLG and BLG when the temperature changes from 113 to 373 K. Here we use the terminology proposed by Ferrari *et al.*[13] for the second-order band at $\sim$2700 cm^{-1}. The extracted values of the temperature coefficients $\chi_{G,2D}$ and zero-temperature frequencies $\omega^0_{G,2D}$ for G and 2D peaks in the spectra from SLG, BLG, and HOPG are summarized in Table I. The absolute values of the 2D peak thermal coefficients are larger that those of G peak. The latter can be related to the fact that the 2D feature is a second-order phonon peak and the shift is enhanced for the

TABLE I. Temperature coefficients for the G and 2D peaks in the single-layer and bilayer graphene.

Material	Peak	χ (cm^{-1}/K)	Peak at 0 K (cm^{-1})	Temperature range (K)
Single-layer graphene	G	−0.016	1584	83–373
Bilayer graphene	G	−0.015	1582	113–373
Highly ordered graphite	G	−0.011	1584	83–373
Single-layer graphene	2D	−0.034	2687	83–373
Bilayer graphene	2D	−0.066	2687	113–373

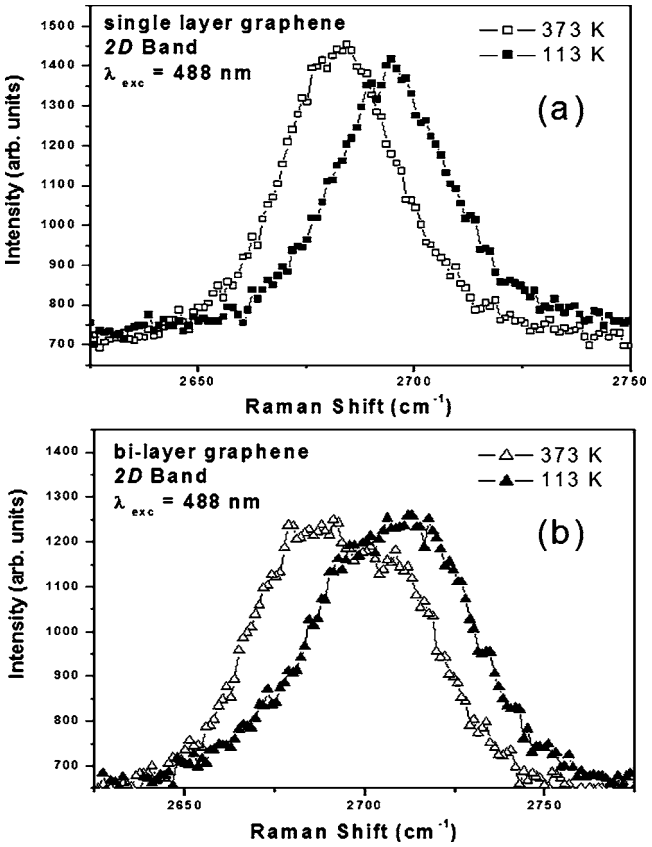

FIG. 3. Raman spectrum showing 2D peak frequency at 113 and 373 K for (a) SLG and (b) BLG.

second harmonic. It is interesting to note that our result for χ_G of the reference HOPG sample exactly coincides with the value reported by Tan *et al.*[27] who also found $\chi_G = -0.011\ \mathrm{cm}^{-1}/\mathrm{K}$. It is rather intriguing that χ_G of SLG is larger than that of BLG and HOPG.

The important conclusion for the nanometrology application of Raman microscopy is that the shift in the G peak position due to the temperature change is comparable to the peak shift with the number of graphene layers n. Gupta *et al.*[14] found that the position of the G band upshifts linearly relative to that of graphite with the increasing $1/n$. The overall shift, as n changes from 19 to a single layer, is $\sim 5-6\ \mathrm{cm}^{-1}$. Our measurements demonstrate that the change in the G peak position as the temperature varied by $\Delta T = 300$ K is about $\sim 4-5\ \mathrm{cm}^{-1}$. The temperature variation of few hundred degrees can occur when the device is cooled for the low temperature measurements or as a result of the increased excitation laser power or application of the realistic bias voltages to the graphene-based devices. The metrology on the basis of 2D band may be more robust with respect to temperature variation since the information about the number of layers is derived mostly from the shape of the 2D feature rather than its position.

This work has been supported, in part, by the DARPA-SRC funded FCRP Center on Functional Engineered Nano Architectonics (FENA) and by the DARPA-DMEA funded UCR-UCLA-UCSB Center for Nanoscience Innovations for Defense (CNID). The authors thank the members of the Nano-Device Laboratory (http://www.ndl.ee.ucr.edu/) for their help with the measurements.

[1] K. S. Novoselov, A. K. Geim, S. V. Morozov, D. Jiang, Y. Zhang, S. V. Dubonos, I. V. Grigorieva, and A. A. Firsov, Science **306**, 666 (2004).
[2] K. S. Novoselov, A. K. Geim, S. V. Morozov, D. Jiang, M. I. Katsnelson, I. V. Grigorieva, S. V. Dubonos, and A. A. Firsov, Nature (London) **438**, 197 (2005).
[3] Y. B. Zhang, Y. W. Tan, H. L. Stormer, and P. Kim, Nature (London) **438**, 201 (2005).
[4] D. A. Abanin, P. A. Lee, and L. S. Levitov, e-print arXiv:cond-mat/0611062.
[5] C. L. Kane and E. J. Mele, Phys. Rev. Lett. **95**, 226801 (2005).
[6] C. L. Kane and E. J. Mele, Phys. Rev. Lett. **95**, 146802 (2005).
[7] D. V. Khveshchenko, Phys. Rev. B **74**, 161402 (2006).
[8] F. Miao, S. Wijeratne, Y. Zhang, U. Coskun, and C. N. Lau, e-print arXiv:cond-mat/0703052.
[9] A. K. Geim and K. S. Novoselov, Nat. Mater. **6**, 183 (2007).
[10] K. Nakada, M. Fujita, G. Dresselhaus, and M. S. Dresselhaus, Phys. Rev. B **54**, 17954 (1996).
[11] L. Brey and H. A. Fertig, Phys. Rev. B **73**, 235411 (2006).
[12] Y. W. Son, M. L. Cohen, and S. G. Louie, Phys. Rev. Lett. **97**, 216803 (2006).
[13] A. C. Ferrari, J. C. Meyer, V. Scardaci, C. Casiraghi, M. Lazzeri, F. Mauri, S. Piscanec, D. Jiang, K. S. Novoselov, S. Roth, and A. K. Geim, Phys. Rev. Lett. **97**, 187401 (2006).
[14] A. Gupta, G. Chen, P. Joshi, S. Tadigadapa, and P. C. Eklund, Nano Lett. **6**, 2667 (2006).
[15] D. Graf, F. Molitor, K. Ensslin, C. Stampfer, A. Jungen, C. Hierold, and L. Wirtz, Nano Lett. **7**, 238 (2007).
[16] A. N. Sidorov, M. M. Yazdanpanah, R. Jalilian, P. J. Ouseph, R. W. Cohn, and G. U. Sumanasekera, Nanotechnology **18**, 135301 (2007).
[17] K. Filippov and A. A. Balandin, MRS Internet J. Nitride Semicond. Res. **8**, 4 (2003).
[18] P. L. Kapitza, J. Phys. (Moscow) **4**, 181 (1941).
[19] K. A. Alim, V. A. Fonoberov, M. Shamsa, and A. A. Balandin, J. Appl. Phys. **97**, 024313 (2005); K. A. Alim, V. A. Fonoberov, and A. A. Balandin, Appl. Phys. Lett. **86**, 053103 (2005).
[20] J. Zou and A. A. Balandin, J. Appl. Phys. **89**, 2932 (2001).
[21] E. P. Pokatilov, D. L. Nika, and A. A. Balandin, Phys. Rev. B **72**, 113311 (2005).
[22] J. Tworzydlo, B. Trauzettel, M. Titov, A. Rycerz, and C. W. J. Beenakker, Phys. Rev. Lett. **96**, 246802 (2006).
[23] C. Postmus, J. R. Ferraro, and S. S. Mitra, Phys. Rev. **174**, 983 (1968).
[24] L. Ci, Z. Zhou, L. Song, X. Yan, D. Liu, H. Yan, Y. Gao, J. Wang, L. Liu, W. Zhou, G. Wang, and S. Xie, Appl. Phys. Lett. **82**, 3098 (2003).
[25] F. Huang, K. T. Yue, P. Tan, S. L. Zhang, Z. Shi, X. Zhou, and Z. Gu, J. Appl. Phys. **84**, 4022 (1998).
[26] H. Herchen and M. A. Cappelli, Phys. Rev. B **43**, 11740 (1991).
[27] P. H. Tan, Y. Deng, Q. Zhao, and W. Cheng, Appl. Phys. Lett. **74**, 1818 (1999).